Mechanical Systems and Signal Processing 40 (2013) 483–498

Contents lists available at ScienceDirect

Mechanical Systems and Signal Processing

journal homepage: www.elsevier.com/locate/ymssp

Dense framelets with two generators and their application in mechanical fault diagnosis

Yi Qin [a,b,*], Jiaxu Wang [b], Yongfang Mao [c]

[a] State Key Laboratory of Mechanical Transmission, Chongqing University, Chongqing 400044, People's Republic of China
[b] School of Manufacturing Science and Engineering, Sichuan University, Chengdu 610065, People's Republic of China
[c] College of Automation, Chongqing University, Chongqing 400044, People's Republic of China

ARTICLE INFO

Article history:
Received 10 April 2013
Received in revised form
8 June 2013
Accepted 11 June 2013
Available online 1 July 2013

Keywords:
Symmetry
Shift-invariance
Signal denoising
Gear fault
Feature extraction

ABSTRACT

Wavelet analysis has been widely applied to mechanical fault diagnosis. Aiming at the problems of current wavelet basis, such as low time–frequency sampling, asymmetry and poor shift-invariance, this paper develops a new family of dense framelets with two generators and some desirable properties. To perform the corresponding framelet transform, three-channel iterated filterbank should be used, where the first and the third channel is decimated while the second channel is undecimated. This arrangement is very helpful for extracting the fault feature of the mid and low frequency band signal components and obtaining some symmetric framelets. To obtain framelets with high symmetry and a specified number of vanishing moments, B-spline and maximally flat linear FIR filter are, respectively, used to design filterbank. Three symmetric framelets and one framelets with symmetric low-pass filter and high-pass filter are constructed. Compared with the higher density framelets and orthonormal wavelets, the proposed framelets have better shift-invariance and denoising performance. Finally, the proposed framelets are applied to fault diagnosis of two gearboxes. The results show that the proposed framelets can be effectively applied to mechanical fault diagnosis and is superior to other commonly-used framelets/wavelets.

1. Introduction

Fault diagnosis of large and complex machines has got great attention in recent decades, in order to keep machines run steadily and prevent economic loss. The mechanical vibration signals usually contain abundant status information of machines. However, due to the harsh working conditions and complex structure, the important fault feature may be embedded in background noise and other normal vibration contents. In many cases, it is very difficult to directly obtain the fault information from the original vibration signals. Especially for low signal-to-noise ratio (SNR) vibration signals, it is greatly necessary for us to develop various effective signal processing methods for different applications.

Currently, the two most commonly used approaches for fault extraction are, respectively, wavelet analysis and empirical mode decomposition (EMD). EMD is a data-driven analyzing approach and possesses wavelet-like filtering characteristic [1,2]. The outstanding merit of EMD is its adaptivity, but it often encounters such problems as mode mixing and ending

* Corresponding author at: Chongqing University, State Key Laboratory of Mechanical Transmission, Sha Pingba, Chongqing 400044, People's Republic of China. Tel.: +86 2365105721.
E-mail address: qy_808@aliyun.com (Y. Qin).

0888-3270/$ - see front matter © 2013 Elsevier Ltd. All rights reserved.
http://dx.doi.org/10.1016/j.ymssp.2013.06.007

effect, and is very sensitive to noise [3]. Due to its good time–frequency localization and "zoom-in" property [4], wavelet analysis does well in signal denoising, singularity detection, weak feature extraction and so on [5]. Thus wavelet analysis is more suitable for processing low SNR vibration signals and extracting transient vibration feature than EMD.

The most widely used wavelet analysis approach may be the discrete wavelet transform (DWT). Daubechies has well established a systematic approach to construct orthonormal wavelets for DWT. To improve the computational efficiency, Sweldens proposed the lifting scheme to construct second generation wavelets [6,7]. DWT and lifting wavelet transform have been well applied to mechanical fault diagnosis [8,9]. Orthonormal wavelets do not have symmetry except for the Harr wavelet, and lack shift-invariance [10]. Besides, DWT has low frequency resolution and energy leakage [11]. These drawbacks limit its effectiveness in some fault extraction applications. Hence, redundant wavelet frames are developed for obtaining such desirable properties as wavelet smoothness, symmetry, high vanishing moments and approximation orders, shift invariance, desirable support, etc. By increasing the number of mother wavelets (generators), more degrees of freedom in the wavelet design can be obtained, and the tight wavelet frames (framelets) with several generators can be constructed by a compactly supported function and oversampled filter bank [12,13]. Daubechies has given the definition of framelets in [12]. The wavelets in overcomplete wavelet transform or frames can be regarded as framelets. Let Ψ be a finite subset of $L^2(\mathbf{R}^d)$, the dyadic wavelet system $X(\Psi)$ generated by the mother wavelets Ψ is given by $\{\psi_{j,k},\ \psi\in\Psi,\ j\in\mathbf{Z}, k\in\mathbf{Z}^d\}$. If $X(\Psi)$ is derived from a multiresolution analysis and is a frame, its elements are named as framelets. To obtain a finer frequency resolution, rational dilation wavelets [14] and overcomplete rational dilation wavelets [15] are proposed. Unfortunately, it is very difficult to design symmetric rational dilation wavelets with FIR filter bank. Using frequency domain method, symmetric overcomplete rational dilation wavelets can be obtained, however the obtained filters without rational transfer functions are less computationally efficient. Ref. [16] has used overcomplete rational dilation discrete wavelets to extract fault feature of gearbox.

Most of the previously developed framelets just offer a redundant representation in the wavelet domain for one signal with respect to time or scale [17–20]. To achieve an oversampling with respect to both time and scale, Selesnick [21] proposes a higher-density discrete wavelet transform. In succession, [22] develops another family of higher-density wavelet frames and apply them to mechanical fault diagnosis. Using the filter structure designed by [21], it is very difficult to obtain symmetric framelets. In order to obtain more symmetric framelets and improve shift-invariance, this paper develops a new family of framelets with dense time–frequency sampling. This type of framelets also consists of two mother wavelets, of which the combined filters are band-pass and high-pass, respectively. Obviously, the proposed framelets also have intermediate scales. However, the wavelet corresponding to the band-pass wavelet filter in this paper is half-integer translated while the wavelet corresponding to the high-pass wavelet filter in [21] is half-integer translated. Obviously, the way in which the proposed wavelet frames here sample the time–frequency plane is different from that in [21]. This arrangement is very helpful for extracting the feature of the mid and low frequency band signal components, because the second channel is undecimated. Since the proposed framelets increase the sampling of time–frequency grid, the proposed framelets are named as dense framelets. Moreover, the new filterbank structure contributes to obtaining more symmetric framelets and increasing the vanishing moments of the second wavelet. Especially, compared to the framelets constructed in [22], the structure forms of band-pass filter and high-pass filter are totally different, thus the new design procedure can lead to constructing three completely symmetric framelets and increasing the vanishing moments of the second wavelet. It is well known that symmetry and shift-invariance are beneficial to signal denoising. The proposed dense framelets have been employed to analyze the faulty gear vibration signal, and the results show that they have better performance on fault feature extraction than Selesnick's framelets and Daubechies wavelets.

2. New dense framelets construction

2.1. Preliminaries

In this paper, the proposed dense framelets sample the time–frequency plane as illustrated in Fig. 1. This arrangement leads to a new filterbank structure which can help us obtain more symmetric framelets and increase the vanishing moments

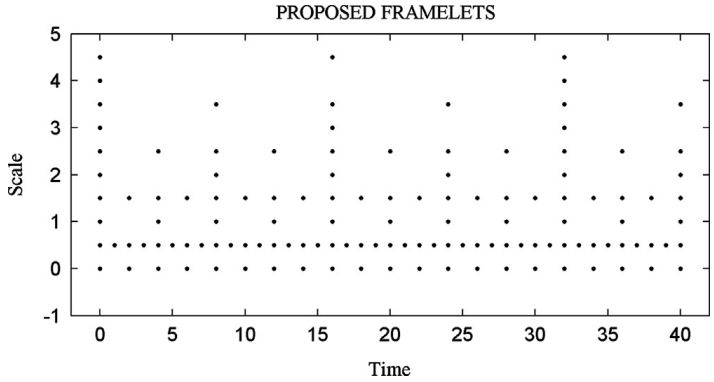

Fig. 1. Sampling of time–frequency plane by the proposed framelets.

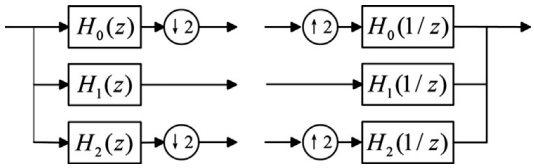

Fig. 2. Iterated decomposition and reconstruction filterbank for the proposed framelets.

of the second wavelet. Moreover, the second channel is undecimated, it may make the proposed framelets be more suitable for extracting the fault feature that are embedded in the mid frequency band component. In order to achieve this time–frequency sampling, the three-channel filterbank illustrated in Fig. 2 is used for signal decomposition and reconstruction. The wavelet filters in the iterated filterbank are denoted by $h_i(n)$ $(i=0,1,2)$. The Z transform $H_i(z)$ and discrete-time Fourier transform $H_i(\omega)$ of $h_i(n)$ are, respectively, given by

$$H_i(z)=\sum h_i(n)z^{-n} \tag{1}$$

$$H_i(\omega)=\sum h_i(n)e^{-j\omega n} \tag{2}$$

From basic multirate identities, the perfect reconstruction (PR) conditions of Fig. 2 are the following:

$$H_0(z)H_0(1/z)+2H_1(z)H_1(1/z)+H_2(z)H_2(1/z)=2 \tag{3}$$

$$H_0(-z)H_0(1/z)+H_2(-z)H_2(1/z)=0 \tag{4}$$

Let $\phi(t)$ be the scaling function, and let $\psi_1(t)$, $\psi_2(t)$ be the two wavelets, using the MRA, the dilation and wavelet equations are defined as

$$\phi(t)=\sqrt{2}\sum_{k\in\mathbf{Z}} h_0(k)\varphi(2t-k) \tag{5}$$

$$\psi_i(t)=\sqrt{2}\sum_{k\in\mathbf{Z}} h_i(k)\phi(2t-k),\quad i=1,\ 2 \tag{6}$$

For $j,k\in\mathbf{Z}$, let

$$\phi_{j,k}(t)=2^{j/2}\phi(2^j t-k) \tag{7}$$

$$\psi_{1,j,k}(t)=2^{j/2}\psi_1(2^j t-k/2) \tag{8}$$

$$\psi_{2,j,k}(t)=2^{j/2}\psi_2(2^j t-k) \tag{9}$$

Then the scaling coefficients and wavelet coefficients can be given by

$$c(j,k)=\langle f(t),\varphi_{j,k}(t)\rangle=\int f(t)\varphi_{j,k}(t)dt \tag{10}$$

$$d_1(j,k)=\langle f(t),\psi_{1,j,k}(t)\rangle=\int f(t)\psi_{1,j,k}(t)dt \tag{11}$$

$$d_2(j,k)=\langle f(t),\psi_{2,j,k}(t)\rangle=\int f(t)\psi_{2,j,k}(t)dt \tag{12}$$

By the iterated filterbank illustrated in Fig. 2, the scaling coefficients and wavelet coefficients at each stage can be fast calculated.

2.2. Filter design

Filter design plays an important role in constructing the dense framelets. In this section, we give our attention to the parameterization of filters $H_0(z)$, $H_1(z)$ and $H_2(z)$. To derive filters h_0, h_1 and h_2 satisfying PR conditions (3) and (4), $H_0(z)$ can be first defined as

$$H_0(z)=\left(\frac{1+z^{-1}}{2}\right)^{K_0}A(z) \tag{13}$$

It is clear that $H_0(z)$ has K_0 roots at $z=-1$. The multiplicity of roots determines the approximation order of the scaling function. Suppose that the degree of $A(z)$ is denoted by M, it then follows that the degree of $H_0(z)$ is denoted by $N=K_0+M$.

To satisfy (4), $H_2(z)$ may be given by

$$H_2(z)=(-z)^{-N+\alpha}H_0(-1/z)=(-z)^{-N+\alpha}\left(\frac{1-z}{2}\right)^{K_0}A(-1/z) \tag{14}$$

where

$$\alpha=\begin{cases}0, & \text{if } N \text{ is odd}\\ -1, & \text{if } N \text{ is even}\end{cases} \tag{15}$$

It follows from (14) that

$$H_0(z)H_0(1/z)=H_2(-z)H_2(-1/z) \tag{16}$$

In order to find $H_2(z)$, spectral factorization should be used. According to (3) and (16), we obtain

$$H_1(z)H_1(1/z)=\frac{1}{2}\left[2-H_0(z)H_0(1/z)-H_2(z)H_2(1/z)\right]=\frac{1}{2}\left[2-H_0(z)H_0(1/z)-H_0(-z)H_0(-1/z)\right] \tag{17}$$

Obviously, $H_1(z)$ can be obtained by spectral factorization if he right-hand side of (16) is nonnegative on the unit circle $z=e^{-j\omega}$. It follows from (16) that $H_0(\omega)$ must satisfy

$$|H_0(\omega)|^2+|H_0(\omega+\pi)|^2\leq 2 \tag{18}$$

In addition, it is easy to note from (17) that the filter coefficient $h_1(n)$ equals zero when n is odd. Therefore, $H_1(z)$ can be written as

$$H_1(z)=\begin{cases}\sum_{n=0}^{(N-1)/2}h_1(2n)z^{-2n}, & \text{if } N \text{ is odd}\\ \sum_{n=0}^{N/2}h_1(2n)z^{-2n}, & \text{if } N \text{ is even}\end{cases} \tag{19}$$

Suppose that $2-H_0(z)H_0(1/z)$ has $2K_2$ ($K_2<K_0$) roots at $z=1$, it then follows from (16) that $2-H_2(-z)H_2(-1/z)$ has $2K_2$ roots at $z=1$. This implies that $2-H_2(z)H_2(1/z)$ has $2K_2$ roots at $z=-1$. Therefore, according to (17), it is easy to note that $H_1(z)H_1(1/z)$ has $2K_2$ roots at $z=1$ and $z=-1$, respectively, which means that $H_1(z)$ has the following form

$$H_1(z)=\left(\frac{1-z^{-1}}{2}\right)^{K_2}\left(\frac{1+z^{-1}}{2}\right)^{K_2}B(z) \tag{20}$$

for some $B(z)$. For convenience, we integrally give the expressions of $H_0(z)$, $H_1(z)$ and $H_2(z)$

$$H_0(z)=\left(\frac{1+z^{-1}}{2}\right)^{K_0}A(z) \tag{21}$$

$$H_1(z)=\left(\frac{1-z^{-1}}{2}\right)^{K_2}\left(\frac{1+z^{-1}}{2}\right)^{K_2}B(z) \tag{22}$$

$$H_2(z)=(-z)^{-N+\alpha}\left(\frac{1-z}{2}\right)^{K_0}A(-1/z) \tag{23}$$

From (21)–(23), it can be seen that $H_0(z)$, $H_1(z)$ and $H_2(z)$ are, respectively, low-pass, band-pass, high-pass filters. Furthermore, the scaling function $\varphi(t)$ has K_0 approximation orders, and the wavelets $\psi_1(t)$ and $\psi_2(t)$, respectively, have K_2 and K_0 vanishing moments. Note that the order of vanishing moments of $\psi_2(t)$ designed in this paper is larger than that of $\psi_2(t)$ designed in [21].

3. Various solutions

In this paper, in order to improve the regularity of framelets and obtain more symmetric framelets, we mainly develop two methods to obtain the solutions of the dense framelets according to (21)–(23). The construction of the proposed framelets begins with the design of wavelet filter $H_0(z)$, which must satisfy (18). Using different methods to design $H_0(z)$, different solutions can be obtained. It is well known that imposing symmetry on $H_0(z)$ will improve the regularity of framelets. Therefore, B-splines and maximally flat low-pass linear-phase FIR filter [23] are, respectively, used to design $H_0(z)$.

3.1. Solutions based on B-splines

Using B-splines, $H_0(z)$ is directly given by

$$H_0(z)=\sqrt{2}\left(\frac{1+z^{-1}}{2}\right)^{K_0} \tag{24}$$

From (24), it is easy to prove that

$$|H_0(\omega)|^2+|H_0(\omega+\pi)|^2=2\left[\left(\cos^2\frac{\omega}{2}\right)^{k_0}+\left(\sin^2\frac{\omega}{2}\right)^{k_0}\right]\leq 2 \tag{25}$$

In such case, since $2-H_0(z)H_0(1/z)$ has two roots at $z=1$, it then follows from (22) and (23) that

$$H_1(z)=\left(\frac{1-z^{-1}}{2}\right)\left(\frac{1+z^{-1}}{2}\right)B(z) \tag{26}$$

$$H_2(z)=(-z)^{-K_0+\alpha}\left(\frac{1-z}{2}\right)^{K_0} \tag{27}$$

where α equals to 0 if K_0 is odd, and α equals to -1 if K_0 is even. According to the discussion in Section 2.2, $B(z)$ will be a constant when $K_0=2,3$. It then follows immediately that all the filters h_0, h_1 and h_2 are symmetric or anti-symmetric. Unfortunately, h_1 cannot be (anti-) symmetric when $K_0>3$. From (26) and (27), we note that the wavelets $\psi_1(t)$ and $\psi_2(t)$ have one and K_0 vanishing moments, respectively. Especially, the second wavelet $\psi_2(t)$ must be symmetric or anti-symmetric.

Example 1. In this example, we set $K_0=2$. From (24), (26) and (27), the filters are given by

$$h_0=\frac{\sqrt{2}}{4}[1,\quad 2,\quad 1,\quad 0]$$

$$h_1=\frac{\sqrt{2}}{4}[1,\quad 0,\quad -1,\quad 0]$$

$$h_2=\frac{\sqrt{2}}{4}[0,\quad -1,\quad 2,\quad -1]$$

with these filters, the scaling function and wavelets are illustrated in Fig. 3. The anti-symmetric wavelet $\psi_1(t)$ and symmetric wavelet $\psi_2(t)$, respectively, have one and two vanishing moments. Using h_0, the Sobolev exponent of the framelets is calculated as 1.5.

Example 2. In this example, we set $K_0=3$. The obtained filter coefficients are listed in Table 1. With these (anti-) symmetric filters, the scaling function $\varphi(t)$ and two wavelets $\psi_1(t)$ and $\psi_2(t)$ are illustrated in Fig. 4. The frequency responses of the filters are illustrated in Fig. 5. It follows from Table 1 that the norms of the filters h_1 and h_2 are, respectively, 0.61 and 0.79. Using h_0, the Sobolev exponent of the framelets is calculated as 2.5. It can be seen from Fig. 4 that the wavelet $\psi_1(t)$ have support 2.5 while the wavelet $\psi_2(t)$ have support 3. Moreover, Fig. 5 shows that h_0, h_1 and h_2 are, respectively, low-pass filter, band-pass filter and high-pass filter.

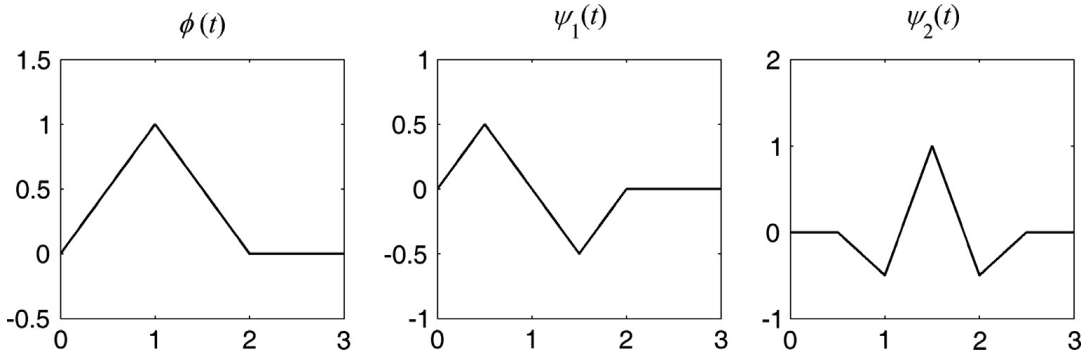

Fig. 3. Symmetric Framelets in Example 1, $K_0=2$.

Table 1
Filter coefficients For Example 2.

n	$h_0(n)$	$h_1(n)$	$h_2(n)$
0	0.176776695297	0.433012701892	0.176776695297
1	0.530330085890	0	−0.530330085890
2	0.530330085890	−0.433012701892	0.530330085890
3	0.176776695297	0	−0.176776695297

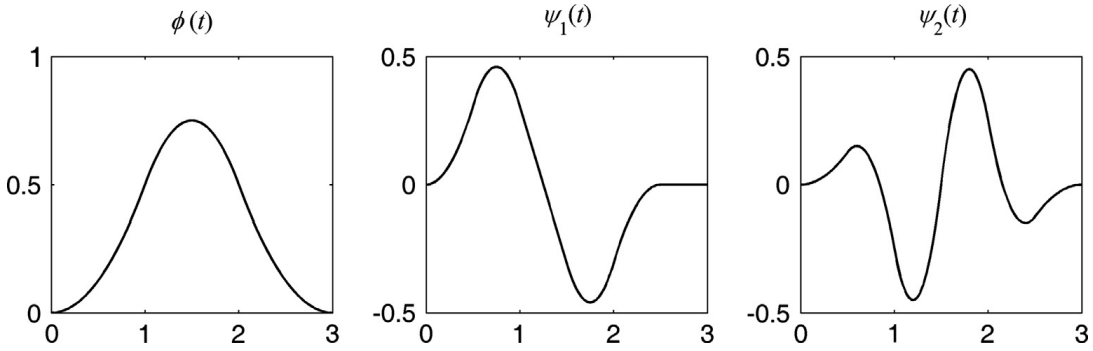

Fig. 4. Symmetric Framelets in Example 2, $K_0=3$.

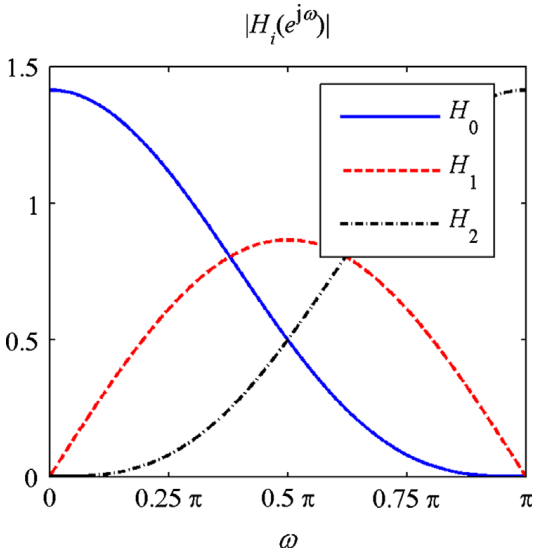

Fig. 5. Frequency responses of h_0, h_1, h_2 in Example 2.

3.2. Solutions based on maximally flat low-pass linear-phase FIR filter

Except for B-splines, the maximally flat low-pass linear-phase FIR filter with symmetry can be used to construct the filter h_0. When K_0 is even and $K_0 \geq 4$, suppose that the filter $H_0(z)$ posses K_0 zeros at $z=-1$, then $H_0(z)$ is given by

$$H_0(z)=\sqrt{2}z^{-K_2+1}\left(\frac{1+z^{-1}}{2}\right)^{K_0}\sum_{k=0}^{K_2-1}\binom{\frac{K_0}{2}+k-1}{k}\left(\frac{-z+2-z^{-1}}{4}\right)^k \tag{28}$$

where $2 \leq K_2 \leq K_0/2$. It is shown in the appendix that $H_0(\omega)$ satisfies (18). From the Proposition 1 in [22], we can know that $2-H_0(z)H_0(1/z)$ has $2K_2$ roots at $z=1$, which means that $H_1(z)$ can be defined as (22). Unfortunately, by the filter $H_0(z)$ defined by (28), we cannot get a symmetric filter $H_1(z)$.

Example 3. In (28), we set $K_0=4$ and $K_2=2$. The scaling function and wavelets are illustrated in Fig. 6. The norms of the filters h_1 and h_2 are, respectively, 0.42 and 0.91, and the Sobolev exponent of the wavelets is 2.44. The wavelet $\psi_1(t)$ has support 6, while the wavelet $\psi_2(t)$ has support 6.5.

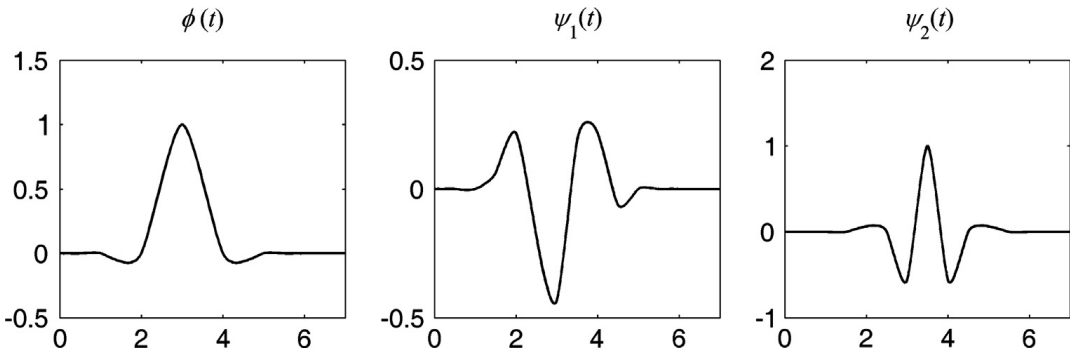

Fig. 6. Framelets in Example 7. $K_2=2$ and $K_0=4$.

Table 2
Filter coefficients for Example 4.

n	$h_0(n)$	$h_1(n)$	$h_2(n)$
0	−0.066291260736	0.121030729569	−0.066291260736
1	0.11048543456	0	−0.11048543456
2	0.662912607362	−0.242061459138	0.662912607362
3	0.662912607362	0	−0.662912607362
4	0.11048543456	0.121030729569	0.11048543456
5	−0.066291260736	0	0.066291260736

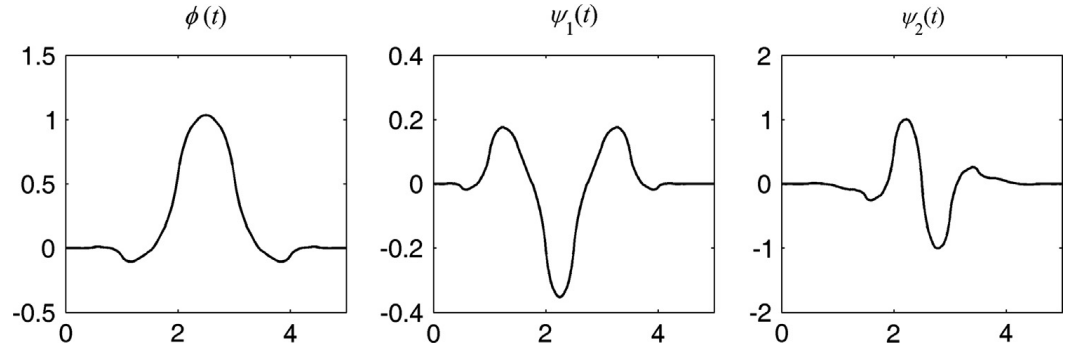

Fig. 7. Symmetric framelets in Example 4, $K_0=3$.

In the following, let us consider such case that K_0 is odd and $K_0\geq 3$. To satisfy (9), using maximally flat low-pass linear-phase even-length FIR filter, $H_0(z)$ can be defined as

$$H_0(z)=\sqrt{2}z^{-1}\left(\frac{1+z^{-1}}{2}\right)^{K_0}\left[1+\frac{K_0}{2}\left(\frac{-z+2-z^{-1}}{4}\right)\right] \tag{29}$$

We can make use of similar method to prove that $H_0(\omega)$ satisfies (18). From the Proposition 2 in [22], it can be seen that $2-H_0(z)H_0(1/z)$ has four roots at $z=1$, which implies $K_2=2$. Note from (29) that the degree of $H_0(z)$ is K_0+2, it then follows from (19) that the degree of $H_1(z)$ is K_0+1. Thus, when $K_0=3$, we can find that $B(z)$ equals to a constant from (22). This implies that the filter $H_1(z)$ is also symmetric. However, when $K_0>3$, it is clear that $B(z)$ cannot be a constant.

Example 4. In (29), we set $K_0=3$. The filter coefficients are listed in Table 2. With these filters, the (anti-) symmetric scaling function and wavelets are obtained, which are illustrated in Fig. 7. The two wavelets, respectively, have two and three vanishing moments. The norms of the filters h_1 and h_2 are, respectively, 0.30 and 0.96. Using the filter h_0, the Sobolev exponent of the wavelets is calculated as 1.65. The wavelet $\psi_1(t)$ has support 4.5, while the wavelet $\psi_2(t)$ has support 5.

Except for the preceding methods, Daubechies filter can be used to design the low pass filter $H_0(z)$, but the obtained filter is very asymmetric. In this paper, we give our main attention to the construction of dense framelets with high symmetry.

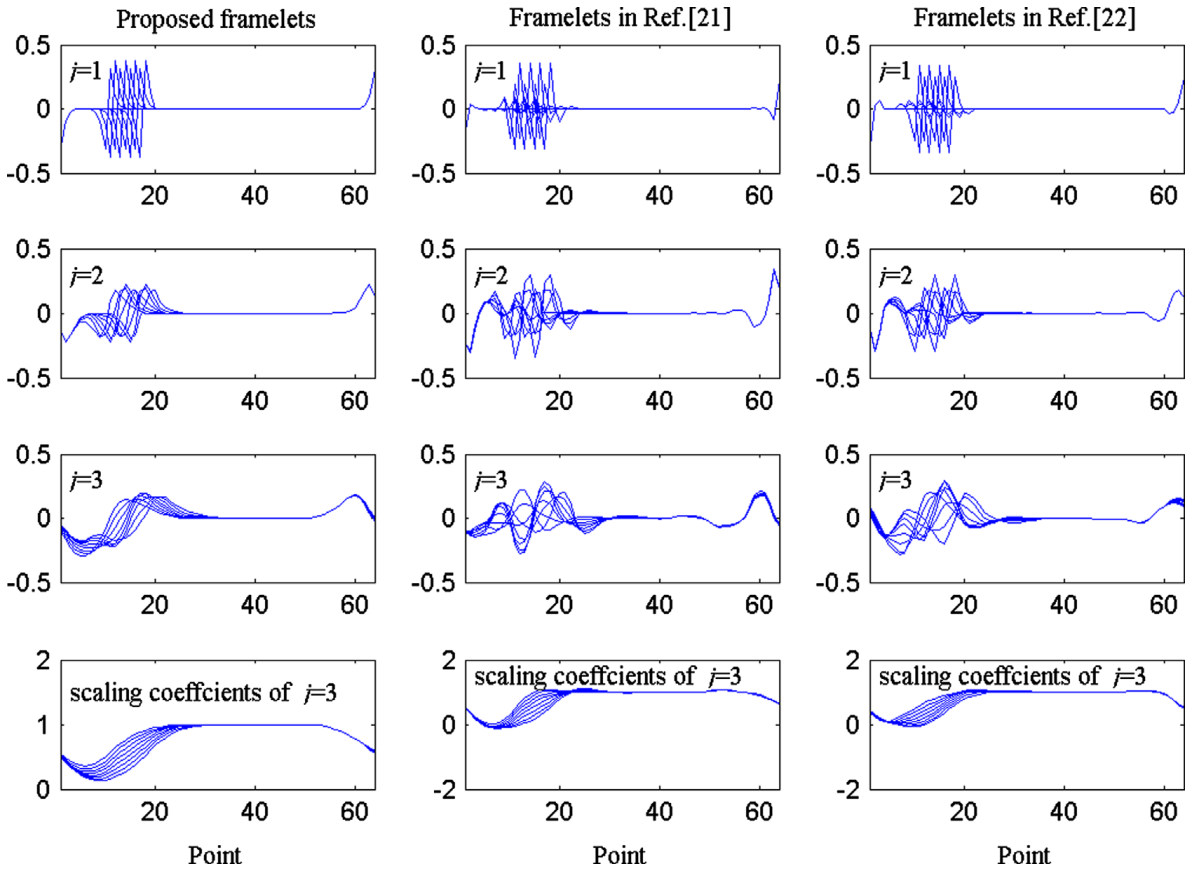

Fig. 8. Reconstruction of $u(n-n_0)$ from coefficients at level j only for three framelets.

4. Comparisons

4.1. Shift invariance

It is well known that small shifts in the input signal can cause major variations in the distribution of energy between wavelet coefficients at different scales if the wavelet transform is not shift invariant. The shift-invariance is important for singular detection and fault feature extraction. In this section, we will discuss the shift-sensitivity property of the proposed framelets and compare them with other framelets. Following the test method introduced in [22], the shift invariance of the proposed framelets can be demonstrated by reconstructing a shifted discrete-time unit step function $u(n-n_0)$ from only its wavelet coefficients at a single scale j. Varying the shift n_0 in increments of 1, the results reveal the shift-varying properties of the wavelet system.

In this experiment, we take $n=0,1,\ldots,63$, $n_0=10,11,\ldots,17$ and three-stages decomposition are performed. Using the wavelet coefficients at level $j=1,2,3$ and the scaling coefficients at level $j=3$, the shift sensitivity of the framelets constructed in Example 2 is illustrated in Fig. 8. Following the same procedure, the framelets with the three vanishing moments constructed in the Example 2 of Ref. [21] and the Example 1 of Ref. [22] are used for comparison, and the results are shown in Fig. 8. From this figure, we can see that the proposed framelets are less shift-sensitive than the framelets constructed by the Selesnick's filterbank structure. Except for the overcomplete filterbank structure, the high symmetry and regularity will be greatly beneficial to shift-invariance. As the proposed framelets have the highest symmetry and regularity, they have the best shift-invariance.

In addition, we can use the energy variance ratio of the wavelet coefficients at each level for the 8 shifted signals to evaluate the shift-invariance of wavelets [22,24]. The energy variance ratio R_j at level j is defined as

$$R_j=\frac{\max\{\sum_i\sum_k d^2_{i,n_0}(j,k)\}}{\min\{\sum_i\sum_k d^2_{i,n_0}(j,k)\}},\quad n_0=10,11,\ldots,17,\quad i=1,2 \tag{30}$$

where $d_{i,n_0}(j,k)$ denotes the wavelet coefficient of the shifted signal $u(n-n_0)$ at level j. The energy variance ratios at levels $j=1,2,3$ obtained by the above three framelets are listed in Table 3. It can be seen from Table 3 that the proposed framelets can obtain very small energy variance ratio, especially at level $j=2,3$. Therefore the proposed framelets has better shift-invariance.

Table 3
Energy variance ratios obtained by the three framelets at levels 1 to 3.

Framelets	Level 1	Level 2	Level 3
Proposed framelets	1.0714	1.0718	1.1291
Framelets in Ref. [21]	1.4375	1.4039	1.6041
Framelets in Ref. [22]	1	1.1519	1.5513

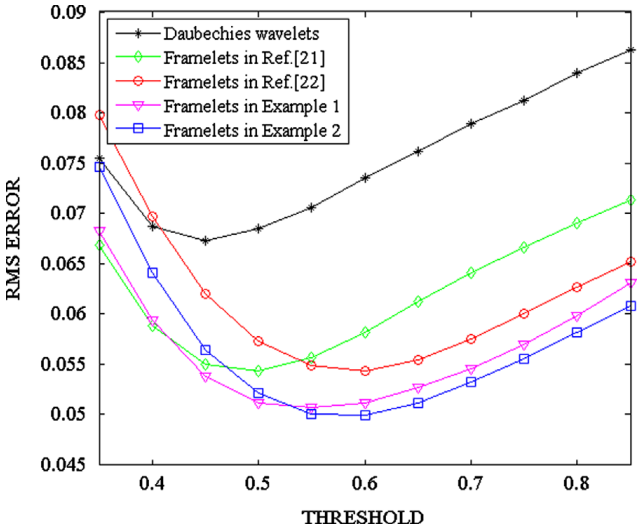

Fig. 9. Comparison of denoising performance for a noisy "Piece-Regular" signal.

4.2. Signal denoising

For a mechanical faulty vibration signal, denoising is a useful and effective method for improving the accuracy of fault detection. Therefore we will compare the denoising performance of the proposed framelets with other typical framelets in this section. The critically-sampled DWT and the undecimated DWT based on the orthonormal Daubechies wavelets with three vanishing moments, the framelets with three vanishing moments constructed in Example 2 of [21], the framelets with three vanishing moments constructed in Example 1 of [22] and the proposed framelets in Examples 1 and 2 of this paper are chosen for the comparison. The Sobolev regularity exponent of the above framelets are, respectively, 1.42, 2.17, 2.44, 1.42 and 1.5. The root-mean-square (RMS) error between the denoised signal and the noisy signal is calculated as a function of the threshold value.

The "Piece-Regular" signal of 1024 points from the WaveLab software package is used for comparison. The signal is normalized so that its maximum value is 1 and an independent white zero-mean Gaussian random noise with the standard derivation of 0.145 is added. For each framelets, we use five stages for the decomposition and reconstruction. When the threshold values range from 0.35 to 0.85, the results obtained from averaging 200 realizations are shown in Fig. 9. It can be seen from Fig. 9 that the proposed framelets in Example 2 have highest denoising performance if the threshold value is larger than 0.5. With the proper threshold (0.6), the best denoising result can be obtained by the framelets constructed in Example 2. Although the framelets constructed in Example 1 has the smallest Sobolev regularity exponent and vanishing moment, its denoising performance approximates to that of the framelets constructed in Example 1 and are higher than other framelets. Obviously, compared with the Sobolev regularity exponent and vanishing moment, symmetry plays a more important role in signal denoising.

5. Application of the proposed framelets to mechanical fault diagnosis

In this section, to demonstrate the effectiveness and superiority, the proposed dense framelets are applied to fault diagnosis. The faulty single stage gearbox and two-stage gearbox will be chosen for fault detection. The gear vibration is mainly generated by the tooth pair meshing effect and the gear rotation. Localized faults, such as broken teeth, cracks and spalls, give sidebands at the tooth meshing frequency and its harmonics on the frequency spectrum. Sidebands are generated by amplitude modulation and/or phase modulation as a result of faulty teeth meshing. When the gear exist an obvious fault, the vibration of the damaged gear is usually represented as impulses. Theoretically, periodic impulses, including the intensity and the time interval, are the robust symptom of tooth damage. However, the useful fault feature may be drowned by noise and normal gear vibration. In order to accurately extract the fault feature, signal denoising or signal decomposition are usually performed. Therefore, the proposed dense framelets are used for fault feature extraction.

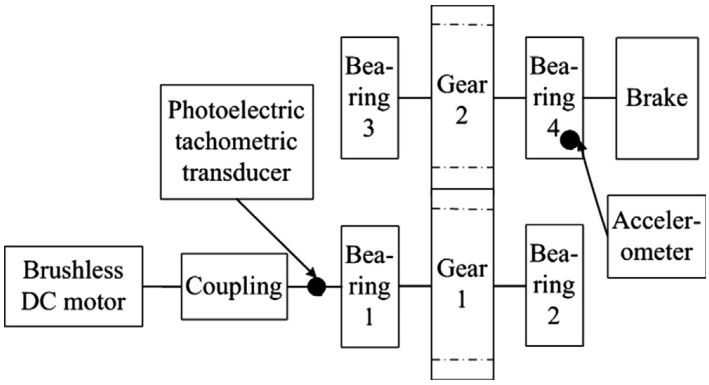

Fig. 10. Schematic sketch of test rig of a faulty single stage gearbox.

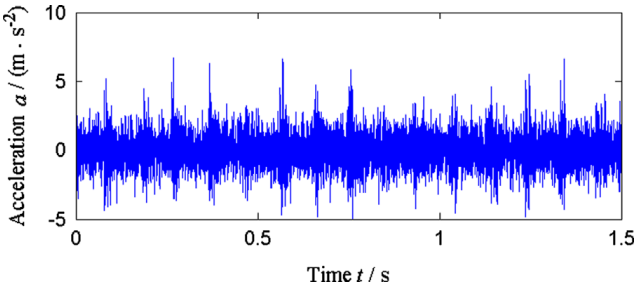

Fig. 11. Vibration acceleration signal of a faulty single stage gearbox.

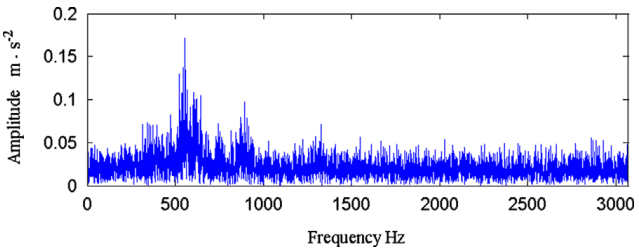

Fig. 12. Frequency spectrum of the vibration signal of a faulty single stage gearbox.

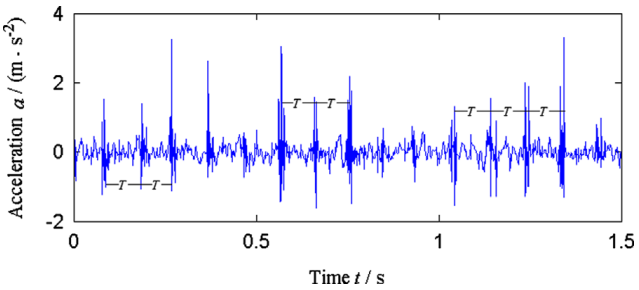

Fig. 13. Denoised vibration signal of a faulty single stage gearbox obtained by the proposed framelets.

5.1. *Fault diagnosis of single stage gearbox*

To perform faulty gear diagnosis experiments, a gearbox rig has been established, whose schematic sketch of is illustrated in Fig. 10. The test rig mainly includes a single stage gearbox, a brushless direct current (DC) motor for driving the gearboxes, coupling and magnetic powder brake for loading. The accelerometer is placed on the gearbox shell, whose position corresponds to that of bearing 2. The gears 1 and 2, respectively, have 34 and 65 teeth. The gear 2 of output shaft has a broken tooth. Using the photoelectric tachometric transducer, the rotating speed of the motor is 1195 rpm, and then the rotating frequency of output shaft (f_{or}) can be calculated as 10.418 Hz. The vibration acceleration signal is sampled at the frequency of 6144 Hz, which is illustrated in Fig. 11. Its frequency spectrum is illustrated in Fig. 12. The impulsive feature is

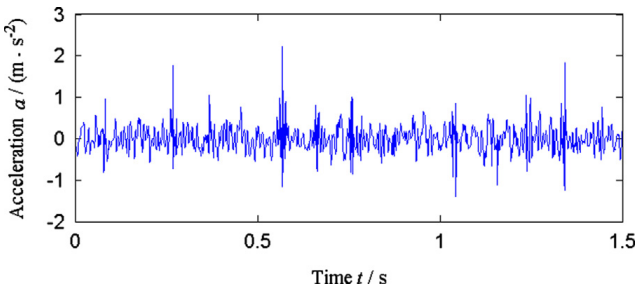

Fig. 14. Denoised vibration signal of a faulty single stage gearbox obtained by the framelets in Example 1 of [22].

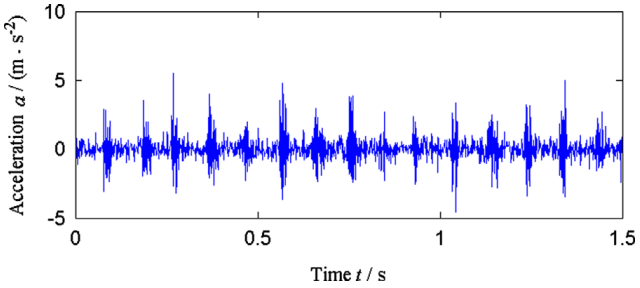

Fig. 15. Denoised vibration signal of a faulty single stage gearbox obtained by Daubechies wavelets.

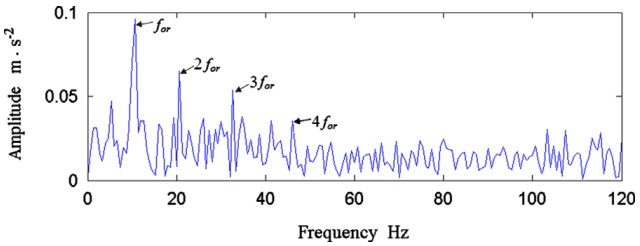

Fig. 16. Envelope spectrum of the denoised signal obtained by the proposed framelets.

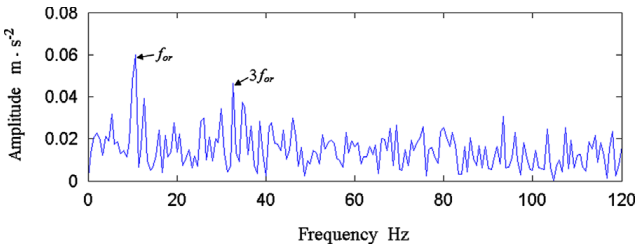

Fig. 17. Envelope spectrum of the denoised signal obtained by the framelets in Example 1 of [22].

not clear in the original vibration signal. Denoising need be performed on this signal to clearly reveal the impulsive component. In the denoising procedure, the thresholding rule is based on the principle of Stein's unbiased risk, and four stages are used. By the framelets constructed in Example 2, the denoised result is shown in Fig. 13. From the figure, we can see that the impulsive period is $T=0.09615$ s, it follows that the impulsive frequency is 10.400 Hz, which is almost equal to the rotating frequency of the output shaft. It immediately implies that there is a fault on the gear 2.

To demonstrate the superiority of the proposed framelets, the framelets with three vanishing moments constructed in Example 1 of [22] and Daubechies wavelets with three vanishing moments are used for comparison. The obtained denoised signals are respectively shown in Figs. 14 and 15. Comparing Fig. 12 with Fig. 13, we can see that the impulses obtained by the framelets in [22] are not clearer than that obtained by the proposed framelets, and even there are not impulses at some time instants. Moreover, comparing Fig. 12 with Fig. 14, we can see that the result obtained by the Daubechies wavelets has lower signal-to-noise ratio even though the impulses are visible. To further demonstrate the superiority of the proposed framelets, the envelope spectra of the denoised signals obtained by the proposed framelets, the framelets in Example 1 of [22] and Daubechies wavelets are, respectively, illustrated in Figs. 16–18. In Fig. 16, there are clear spectral lines at impulsive

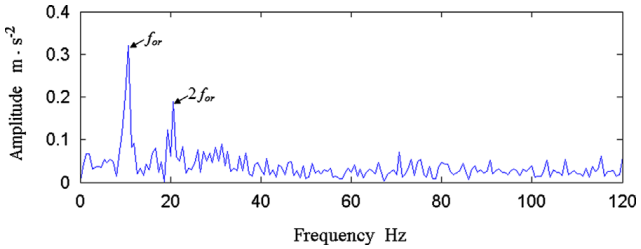

Fig. 18. Envelope spectrum of the denoised signal obtained by Daubechies wavelets.

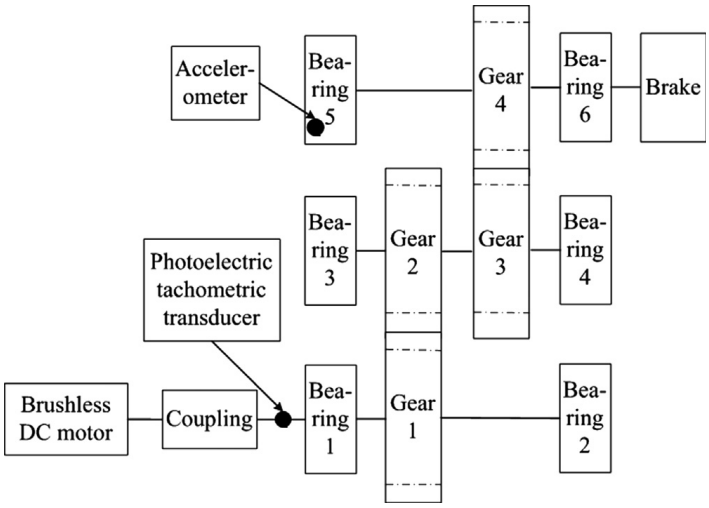

Fig. 19. Schematic sketch of test rig of a faulty two-stage gearbox.

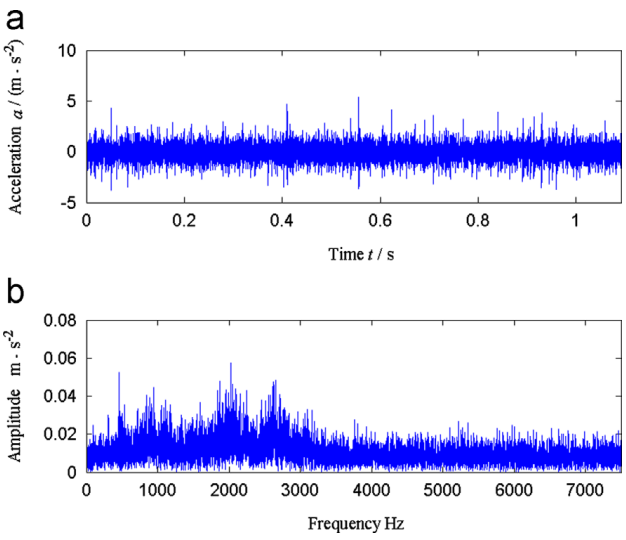

Fig. 20. Vibration acceleration signal of a faulty two-stage gearbox and its frequency spectrum: (a) time-domain waveform and (b) frequency spectrum.

frequency (f_{or}) and its multiple frequency ($2f_{or}$, $3f_{or}$, $4f_{or}$), which is better consistent with the envelope spectrum structure of an impulsive vibration component. For comparison, in Fig. 17, there only are clear spectral lines at f_{or} and $3f_{or}$. Similarly, there only are clear spectral lines at f_{or} and $2f_{or}$ in Fig. 18. It then follows immediately that the proposed dense framelets are more suitable for extracting impulsive feature of faulty gear.

5.2. Fault diagnosis of two-stage gearbox

To further validate the effectiveness of the proposed framelets in mechanical fault diagnosis, another experiment is performed to detect the fault of a two-stage gearbox. We adopt the similar test rig, whose schematic sketch of test rig is illustrated in Fig. 19. The accelerometer is placed on the gearbox shell, whose position corresponds to that of bearing 5.

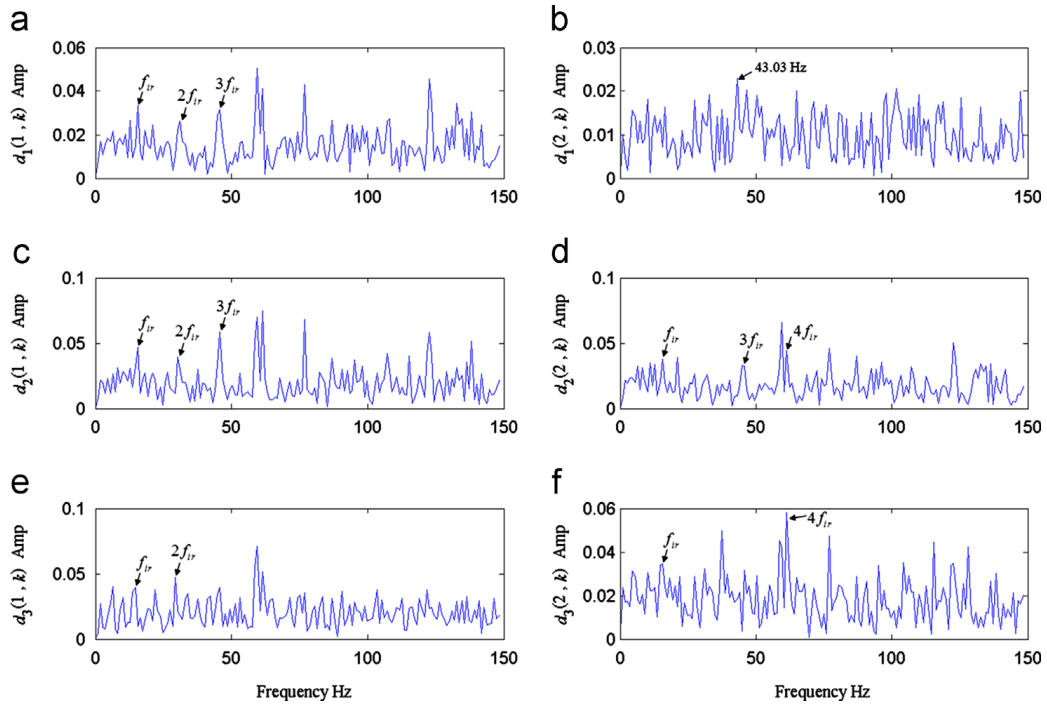

Fig. 21. Envelope spectra of wavelet coefficients at each level obtained by the proposed framelets: (a) mid-frequency wavelet coefficients at level 1, (b) high-frequency wavelet coefficients at level 1, (c) mid-frequency wavelet coefficients at level 2, (d) high-frequency wavelet coefficients at level 2, (e) mid-frequency wavelet coefficients at level 3 and (f) high-frequency wavelet coefficients at level 3.

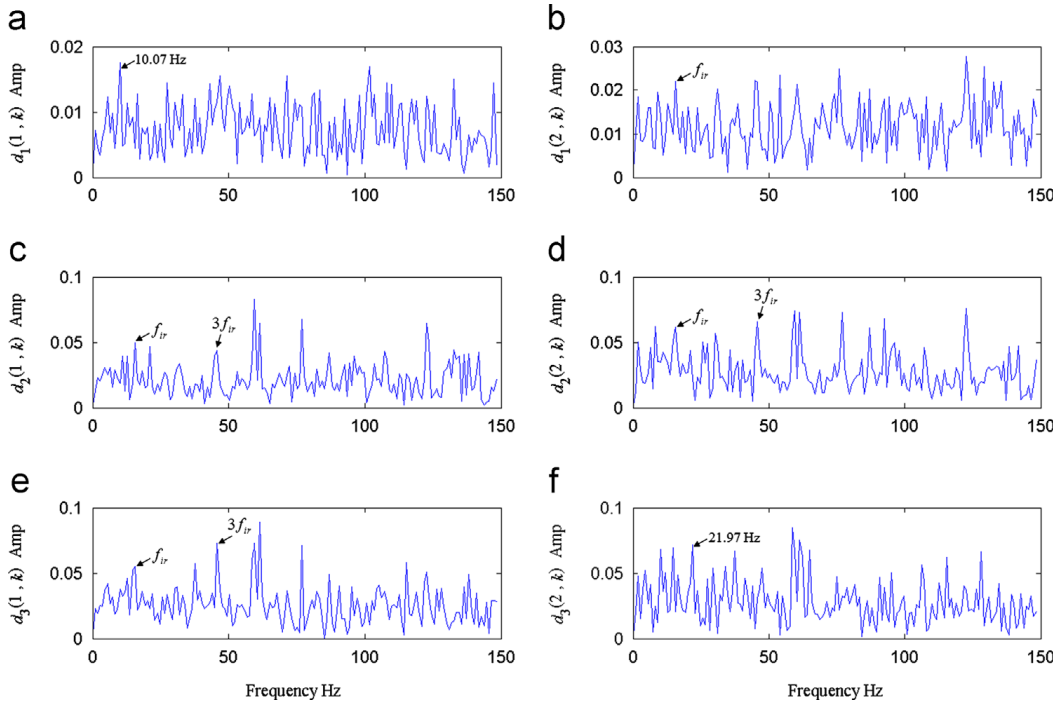

Fig. 22. Envelope spectra of wavelet coefficients at each level obtained by the framelets in Example 1 of [22]: (a) mid-frequency wavelet coefficients at level 1, (b) high-frequency wavelet coefficients at level 1, (c) mid-frequency wavelet coefficients at level 2, (d) high-frequency wavelet coefficients at level 2, (e) mid-frequency wavelet coefficients at level 3 and (f) high-frequency wavelet coefficients at level 3.

In the experimental two-stage gearbox, the teeth numbers of gears 1, 2, 3, 4 are, respectively, 30, 69, 18 and 81. The gear 1 of input shaft has spalls. By measurement with the photoelectric tachometric transducer, the rotating speed of the motor is 908 rpm, i.e. the rotating frequency of input shaft f_{ir} can be calculated as 15.133 Hz. The vibration acceleration signal is sampled at the frequency of 15,000 Hz, which is illustrated in Fig. 20(a). Its frequency spectrum is also illustrated in Fig. 20(b). Since the spalling fault is weaker than the fault of broken teeth, we cannot see impulsive feature in the time waveform of vibration signal. Therefore, we perform three-stage decomposition on the acquired vibration signal with the framelets constructed in Example 2, and then calculate the envelope spectra of wavelet coefficients at each level. The

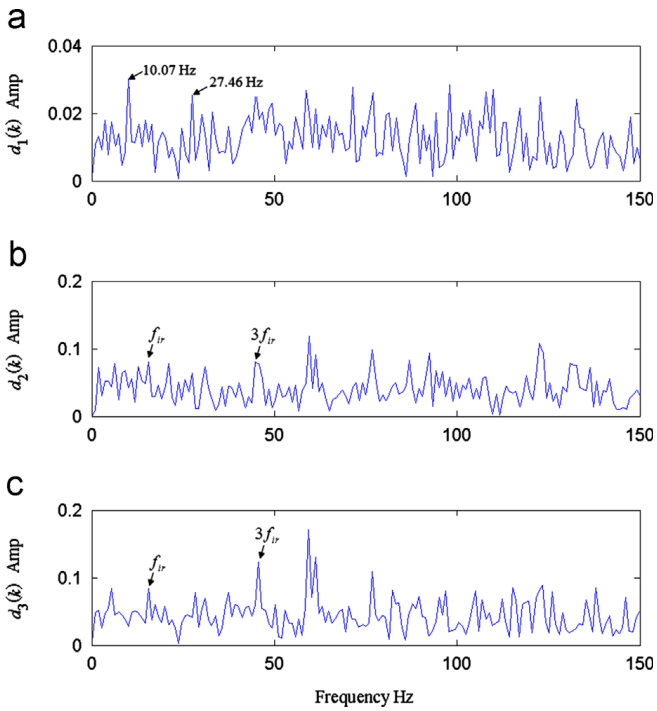

Fig. 23. Envelope spectra of wavelet coefficients at each level obtained by Daubechies wavelets: (a) wavelet coefficients at level 1, (b) wavelet coefficients at level 2, (c) wavelet coefficients at level 3.

obtained results are illustrated in Fig. 21. From this figure, we can see that there are obvious spectral lines at the fault characteristic frequency (f_{ir}) and its frequency multiplication in both envelope spectra of mid-frequency wavelet coefficients and envelope spectra of high-frequency wavelet coefficients. Note in particular that in Fig. 21(a) and (c), there are clear spectral lines at impulsive frequency (f_{ir}) and its multiple frequency ($2f_{ir}$, $3f_{ir}$), which well indicate the gear fault of the input shaft. Comparing Fig. 21(a), (c) and (e) with Fig. 21(b), (d) and (f), the envelope spectra of mid-frequency wavelet coefficients reveal more obvious fault characteristic frequencies than the envelope spectra of high-frequency wavelet coefficients. This is mainly because that the faulty components are located at the mid-frequency wavelet coefficients and the second channel is undecimated. The characteristic frequencies in Fig. 21(a) and (c)–(f) provide sufficient evidence for the existence of gear fault of the input shaft.

Similarly, following the same procedure, the framelets with three vanishing moments constructed in Example 1 of [22] and Daubechies wavelets with three vanishing moments are used for analyzing the same signal, and the obtained results are, respectively, illustrated in Figs. 22 and 23. In Fig. 22(b), there is a peak value at f_{ir}, but this spectral line is not more remarkable comparing with the adjacent spectral line with peak value. In Fig. 22(c)–(e), there are spectral lines at f_{ir} and $3f_{ir}$, however the spectral line at $2f_{ir}$ is not obvious. In Fig. 23(b) and (c), there are spectral lines at f_{ir} and $3f_{ir}$, but the spectral line at f_{ir} is not remarkable, which may affect the accuracy of fault identification. Furthermore, comparing Figs. 21–23, we can see that there are the most spectral lines at the fault characteristic frequency (f_{ir}) and its frequency multiplication in Fig. 21. With more spectral lines at characteristic frequencies, the fault identification will be more accurate and reliable. It follows that the proposed framelets have better performance in analyzing such faulty vibration signals.

In conclusion, using the proposed framelets, the gearbox fault can be more reliably and accurately identified.

6. Conclusion

Aiming at the limitations of current wavelet analysis in mechanical fault feature extraction, this paper has developed a new family of dense framelets with high symmetry and a specified number of vanishing moments. In the iterated filterbank, the second channel is undecimated while the third channel is decimated. With the new filter bank, we can construct more symmetric framelets, improve the shift-invariance and increase the vanishing moments of the second wavelet. Therefore, the proposed framelets is very suitable for signal denoising and extracting the feature of the mid and low frequency band signal. Using B-spline and maximally flat linear FIR filter, two design methods are proposed to obtain various solutions, then three symmetric framelets and one framelets with symmetric low-pass filter and high-pass filter are constructed. Comparing with higher density framelets and orthonormal wavelets, the proposed framelets have better shift-invariance and denoising performance. Based on the constructed framelets, the faults of two gearboxes are effectively recognized and the diagnostic results are superior to those obtained by higher density framelets and orthonormal wavelets.

If we relax the tightness of the wavelet frame, nontight symmetric wavelet frames can also be constructed by employing dual wavelet frames techniques. In addition, the dual-tree dense framelet transform is worth investigating for the vibration signal decomposition and demodulation.

Acknowledgments

The support by National Natural Science Foundation of China (nos. 50905191 and 51005262) and China Postdoctoral Science Foundation funded project (no. 2012M521690) for this research is gratefully acknowledged.

Appendix

By the frequency response of (28), we have

$$|H_0(\omega)|^2 = 2\left(\cos^2\frac{\omega}{2}\right)^{K_0}\left[\sum_{k=0}^{K_2-1}\binom{\frac{K_0}{2}+k-1}{k}\left(\sin^2\frac{\omega}{2}\right)^k\right]^2 \tag{31}$$

$$|H_0(\omega+\pi)|^2 = 2\left(\sin^2\frac{\omega}{2}\right)^{K_0}\left[\sum_{k=0}^{K_2-1}\binom{\frac{K_0}{2}+k-1}{k}\left(\cos^2\frac{\omega}{2}\right)^k\right]^2 \tag{32}$$

Define

$$h(k) = \binom{\frac{K_0}{2}+k-1}{k}, \quad k = 0, 1, \ldots, K_2-1$$

$$Q_1(\omega) = \left[\sum_{k=0}^{K_2-1}\binom{\frac{K_0}{2}+k-1}{k}\left(\sin^2\frac{\omega}{2}\right)^k\right]^2$$

$$Q_2(\omega) = \left[\sum_{k=0}^{K_2-1}\binom{\frac{K_0}{2}+k-1}{k}\left(\cos^2\frac{\omega}{2}\right)^k\right]^2$$

Let $x = \cos^2(\omega/2)$, then we can write

$$Q_1(\omega) = \sum_{n=0}^{2K_2-2} q_1(n)(1-x)^n$$

$$Q_2(\omega) = \sum_{n=0}^{2K_2-2} q_2(n)x^n$$

where $q_1(n) = q_2(n) = h \times h(n)$. It follows from (31) and (32) that

$$\frac{1}{2}\left[|H_0(\omega)|^2 + |H_0(\omega+\pi)|^2\right] = x^{K_0}\sum_{n=0}^{2K_2-2} q(n)(1-x)^n + (1-x)^{K_0}\sum_{n=0}^{2K_2-2} q(n)x^n \tag{33}$$

Also let

$$p(n) = \binom{K_0+n-1}{n}$$

From the Proposition 1 in [22], we have

$$q(n) = p(n), \; n \le K_0-1$$

$$q(n) < p(n), \; n > K_0-1$$

As $2K_2-2 < K_0-1$, it is clear that

$$x^{K_0}\sum_{n=0}^{2K_2-2} q(n)(1-x)^n + (1-x)^{K_0}\sum_{n=0}^{2K_2-2} q(n)x^n < x^{K_0}\sum_{n=0}^{K_0-1} p(n)(1-x)^n + (1-x)^{K_0}\sum_{n=0}^{K_0-1} p(n)x^n = 1 \tag{34}$$

It follows from (33) and (34) that

$$|H_0(\omega)|^2 + |H_0(\omega+\pi)|^2 < 2$$

References

[1] N.E. Huang, Z. Shen, S.R. Long, The empirical mode decomposition and Hilbert spectrum for nonlinear and non-stationary time series analysis, Proc. R. Soc. London, Ser. A 454 (1998) 903–995.
[2] P. Flandrin, G. Rilling, P. Goncalves, Empirical mode decomposition as a filter bank, IEEE Signal Process. Lett. 11 (2) (2004) 112–114.
[3] R.T. Rato, M.D. Ortigueira, A.G. Batista, On the HHT, its problems, and some solutions, Mech. Syst. Sig. Process. 22 (2008) 1374–1394.
[4] I. Daubechies, Ten Lectures on Wavelets, SIAM, Philadelphia, PA, 1992.
[5] Z.K. Peng, F.L. Chu, Application of the wavelet transform in machine condition monitoring and fault diagnostics: a review with bibliography, Mech. Syst. Sig. Process. 18 (2004) 199–221.
[6] W. Sweldens, The lifting scheme: a custom-design construction of biorthogonal wavelets, Appl. Comput. Harmon. Anal. 3 (2) (1996) 186–200.
[7] The lifting scheme: A construction of second generation wavelets. SIAM J. Math. Anal. 29(2): 511–546.
[8] L.X. Gao, Z.J. Yang, L.G. Cai, et al., Roller bearing fault diagnosis based on nonlinear redundant lifting wavelet packet analysis, Sensors 11 (1) (2011) 260–277.
[9] H.K. Jiang, Z.J. He, C.D. Duan, et al., Gearbox fault diagnosis using adaptive redundant lifting scheme, Mech. Syst. Sig. Process. 20 (8) (2006) 1992–2006.
[10] N. Kingsbury, Complex wavelets for shift invariant analysis and filtering of signals, Appl. Comput. Harmon. Anal. 10 (3) (2000) 234–253.
[11] Z.K. Peng, M.R. Jackson, J.A. Rongong, et al., On the energy leakage of discrete wavelet transform, Mech. Syst. Sig. Process. 23 (2) (2009) 330–343.
[12] I. Daubechies, B. Han, A. Ron, Z. Shen, Framelets: MRA-based constructions of wavelet frames, Appl. Comput. Harmon. Anal. 14 (1) (2003) 1–46.
[13] C.K. Chui, W. He, J. Stöcklerckler, Compactly supported tight and sibling frames with maximum vanishing moments, Appl. Comput. Harmon. Anal. 13 (3) (2002) 224–262.
[14] T. Blu, Iterated filter banks with rational rate changes-connection with discrete wavelet transforms, IEEE Trans. Signal Process. 41 (12) (1993) 3232–3244.
[15] I. Bayram, I.W. Selesnick, Frequency-domain design of overcomplete rational-dilation wavelet transforms, IEEE Trans. Signal Process. 57 (8) (2009) 2957–2972.
[16] B. Chen, Z. Zhang, C. Sun, et al., Fault feature extraction of gearbox by using overcomplete rational dilation discrete wavelet transform on signals measured from vibration sensors, Mech. Syst. Sig. Process. 33 (2012) 275–298.
[17] I.W. Selesnick., The double density DWT, in: A. Petrosian, F.G. Meyer (Eds.), Wavelets in Signal and Image Analysis: From Theory to Practice, Kluwer Academic, 2001.
[18] B. Han, Q. Mo, Symmetric MRA tight wavelet frames with three generators and high vanishing moments, Appl. Comput. Harmon. Anal. 18 (1) (2005) 67–93.
[19] B. Dong, Z.W. Shen, Pseudo-splines, wavelets and framelets, Appl. Comput. Harmon. Anal. 22 (1) (2007) 78–104.
[20] B. Han, Construction of wavelets and framelets by the projection method, Int. J. Math. Sci. 1 (2008) 1–40.
[21] I.W. Selesnick, A higher density discrete wavelet transform, IEEE Trans. Signal Process. 54 (8) (2006) 3039–3048.
[22] Y. Qin, J.X. Wang, B.P. Tang, Y.F. Mao, Higher density wavelet frames with symmetric low-pass and band-pass filters, Signal Process. 90 (12) (2010) 3219–3231.
[23] O. Herrmann, On the approximation problem in nonrecursive digital filter design, IEEE Trans. Circuits Theory 18 (3) (1971) 411–413.
[24] N.G. Kingsbury, Shift invariant properties of the dual-tree complex wavelet transform, in: Proceedings of ICASSP 99, Phoenix, AZ, 1999, pp. 1221–1224.